I too ♥ I_2

Ellen Kuhl[†] and Alain Goriely[‡]

[†]*Department of Mechanical Engineering, Stanford University, Stanford, CA-94305, United States,*
[‡]*Mathematical Institute, University of Oxford, Oxford, UK*

February 2024

Abstract

In contemporary elasticity theory, the strain energy density function predominantly relies on the first invariant, I_1, of the strain tensor, particularly influenced by models derived from rubber elasticity. This traditional focus has facilitated significant advancements in understanding and modeling the elastic behavior of various materials under compression and tension. However, this approach may not fully capture the complexities of materials exhibiting pronounced shear deformations, such as very soft biological tissues. This paper explores the implications and potential benefits of constitutive models where the strain energy density function is exclusively a function of the second invariant, I_2. By shifting the focus towards I_2, we aim to address the limitations of current models in accurately describing shear-dominated behaviors and to provide a more comprehensive understanding of material responses, particularly for materials that do not conform to the assumptions underlying I_1-centric theories. Through analytical musings, data analysis, and automated model discovery we investigate the feasibility of this approach and its consequences for predicting material behavior under various loading conditions. We show that the so-called "G materials" conforming to I_2-only have interesting properties that are found in biological tissues and are fundamentally different from the traditional elastomeric materials.

1 Introduction

In the field of elasticity, constitutive modeling plays a pivotal role in predicting the material response under various deformation conditions. The core of such modeling lies in the formulation of strain-energy functions, which are scalar fields representing the stored energy per unit volume in a material. To accurately describe the mechanical behavior of such hyperelastic materials, these functions have traditionally been constructed from the invariants of the deformation gradient tensor. Invariants are unique scalar quantities derived from the deformation gradient; they remain unchanged under any coordinate transformation, thus providing an objective measure of deformation. The primary invariants typically employed are the first, second, and third invariants of the right Cauchy-Green deformation tensor. By leveraging these invariants, constitutive models can encapsulate the material's response to external forces or deformations and ensure that the stress-strain relationships are framed in an invariant manner, satisfying both material objectivity and the laws of thermodynamics [31, 13]. This invariant-based approach forms the foundation of hyperelastic material modeling, offering a rigorous and robust framework for simulating the complex behavior of materials under mechanical loads.

In this context, it is well appreciated that the second invariant of the strain tensor, I_2, represents an underutilized yet significant component in the theoretical framework of elasticity [18, 2]. Despite its fundamental role in characterizing the deformation state of a material, particularly in describing the shape change independent of volume change, I_2 has not been sufficiently integrated into elasticity theory and its applications [1]. This oversight may stem from the historical focus on simpler deformation models or analytical challenges in incorporating I_2 into existing frameworks. However, the inclusion of I_2 is crucial for a more comprehensive understanding of material behavior, especially in describing the properties of biological soft tissues under complex loading scenarios where deformation cannot be accurately described by the first invariant I_1 alone.

Exploring a theory of elasticity primarily focused on the second invariant, I_2, presents a compelling new research direction, particularly for addressing the mechanical behavior of very soft biological materials, for example from the brain or arteries. These materials exhibit complex mechanical properties, that traditional elasticity theories, which predominantly concentrate on the first invariant, I_1, may not adequately capture. For instance, many such materials exhibit the reverse Poynting effect [27, 28]. Therefore, the distinctive deformation characteristics of soft biological tissues, marked by pronounced shape changes with minimal volume change, highlight the relevance of I_2 in accurately describing their mechanical responses, especially under shear [10].

While many authors have emphasised the need to include the second invariant to obtain a better characterisation of a material, here, we go one step further and consider the consequences of a theory based *solely* on the second invariant. The reason for this choice is twofold. First the systematic system identification of data sets for a variety of samples lead to the puzzling finding, against all common practice, that some materials are better represented by a strain-energy function that only depends on I_2. Second, by taking the limit to I_2-only materials theoretically, we can gain a better understanding of the effect of the second invariant on the properties of tissues and improve our understanding of isotropic incompressible hyperelastic materials.

2 Background and definitions

We consider a solid subject to a deformation $\mathbf{x} = \boldsymbol{\chi}(\mathbf{X})$, which maps material points $\mathbf{X}$ in the reference configuration to points $\mathbf{x}$ in the current configuration (see [14] for reference). Then the deformation gradient tensor, that measures changes between the two configurations is

$$\mathbf{F} = \mathrm{Grad}(\boldsymbol{\chi}) = \frac{\partial \mathbf{x}}{\partial \mathbf{X}}. \tag{1}$$

The left Cauchy-Green deformation tensor $\mathbf{B}$ is related to the deformation gradient tensor by $\mathbf{B} = \mathbf{F}\mathbf{F}^{\mathsf{T}}$, where $\mathbf{F}^{\mathsf{T}}$ is the transpose of $\mathbf{F}$. This tensor characterizes the local deformation of the material and is used to define the invariants of deformation, which are scalar quantities invariant under coordinate transformations. The principal invariants of $\mathbf{B}$ are:

$$I_1 = \mathrm{tr}(\mathbf{B}), \tag{2}$$

$$I_2 = \frac{1}{2}\left[(\mathrm{tr}(\mathbf{B}))^2 - \mathrm{tr}(\mathbf{B}^2)\right], \tag{3}$$

$$I_3 = \det(\mathbf{B}), \tag{4}$$

where $\mathrm{tr}(\mathbf{B})$ is the trace of $\mathbf{B}$, and $\det(\mathbf{B})$ is the determinant of $\mathbf{B}$.

The invariants of the left Cauchy-Green deformation tensor B, can also be expressed in terms of the *principal stretches* $\{\lambda_1, \lambda_2, \lambda_3\}$ which are the square roots of the eigenvalues of $\mathbf{B}$:

$$I_1 = \lambda_1^2 + \lambda_2^2 + \lambda_3^2, \tag{5}$$

$$I_2 = \lambda_1^2\lambda_2^2 + \lambda_2^2\lambda_3^2 + \lambda_1^2\lambda_3^2, \tag{6}$$

$$I_3 = \lambda_1^2\lambda_2^2\lambda_3^2. \tag{7}$$

In the particular case where the motion is *isochoric*, $I_3 = 1$, the second invariant can be written $I_2 = \lambda_1^{-2} + \lambda_2^{-2} + \lambda_3^{-2}$.

2.1 Geometric interpretation of the three invariants

The invariants are not only algebraic objects that emerge from the analysis of the strain tensors, they also have a natural geometric interpretation [4, 19, 26].

We start with the easy one, the third invariant of the deformation tensor, I_3, which measures *the relative volume change of a material element during deformation*. If I_3 is greater than 1, the material element has expanded, and if I_3 is less than 1, it has contracted. Hence, I_3 provides a scalar measure of the volumetric dilation or compression of a material element due to deformation.

It is also relatively easy to interpret the first invariant of the deformation tensor, I_1. Geometrically, I_1 represents the *sum of the squared stretches of an infinitesimal line element averaged over all possible orientations within the material*. This invariant does not depend on the specific directions of stretching but rather gives a measure that is the same regardless of the coordinate system. In the classical theory of rubber elasticity, this is particularly significant as it simplifies the complex molecular chain network of rubber into a single scalar quantity that represents the average stretch between crosslinks in the network. The averaging process inherent to I_1 allows for the consideration of stretches in all directions, providing a scalar measure of deformation that is a fundamental building block for constitutive models of isotropic hyperelastic materials based on the elongation of molecular chains.

The second invariant, however, is harder to interpret. Nevertheless, I_2, can be geometrically interpreted as *three times the square of the stretch ratio of an infinitesimal area element averaged over all possible orientations* [19]. Therefore, this invariant takes into account changes in shape that an area element undergoes during deformation, excluding any changes in volume. To compute I_2, one can consider an infinitesimal area oriented in a Cartesian coordinate system that undergoes deformation. The components of the line segment defining the area stretch by ratios corresponding to the principal stretches, and I_2 captures the average of the product of any two distinct stretches across all orientations. This averaging process considers the area element's orientations in the deformed state and quantifies the extent of shear deformation. Therefore, the importance of I_2 is particularly pronounced in the analysis of materials that undergo large shear deformations.

2.2 Constitutive models

The strain-energy density function W is a scalar function that quantifies the elastic energy stored in a material due to deformation. For hyperelastic materials, which are ideal elastic materials that return to their original shape upon unloading, W is solely a function of the three strain invariants $W = W(I_1, I_2, I_3)$. In the case of incompressible materials, such as rubber, the volume is conserved during deformation, implying that $I_3 = 1$ always holds true. For such materials, the strain-energy density function can be simplified to depend only on I_1 and I_2, as $W = W(I_1, I_2)$, since I_3 remains constant.

The Cauchy stress tensor $\mathbf{T}$, which represents the internal forces in the material, can be derived from the strain-energy density function for an isotropic, hyperelastic material using the well-known representation formula:

$$\mathbf{T} = -p\mathbf{1} + 2\frac{\partial W}{\partial I_1}\mathbf{B} - 2\frac{\partial W}{\partial I_2}\mathbf{B}^{-1}, \tag{8}$$

where p is the Lagrange multiplier enforcing the incompressibility constraint, $\det(\mathbf{F}) = 1$, and $\mathbf{1}$ is the identity tensor. In the absence of body forces, the equilibrium of the material is described by

$$\operatorname{div} \mathbf{T} = \mathbf{0}, \tag{9}$$

where div is the divergence operator with respect to $\mathbf{x}$, ensuring that the net force on any part of the material is zero. The determination of the appropriate form of W is a central problem in the theory of elasticity since there is no general theory that provides its functional form based on first principles. Different choices for W lead to quantitative and qualitative differences in the material response.

The starting point of most studies is the *neo-Hookean model*. It offers a simple yet powerful description of the elastic behavior of rubbery materials at finite deformation. It is simply given by

$$W = C_1(I_1 - 3), \tag{10}$$

where $C_1 = E/6$ is related to the small-strain Young's modulus E. This modulus can be connected to molecular-level phenomena, thus allowing the macroscopic mechanical properties to be related to the microstructure of the material [7].

The *generalized neo-Hookean* (GnH) model extends this concept by imposing that W depends only on the first invariant I_1 which simplifies both the choice of possible functional forms and hence model fitting, and the mathematical treatment of these materials. However, this choice also implies a focus on the compressive and tensile material behaviors and assumes a microscopic model based on affine deformations. It implies that energy is stored only in chain extension and compression [11].

In contrast, the *Mooney-Rivlin model* [30, 37], was one of the first to incorporate I_2-dependent terms, which significantly improved the agreement between theory and experiments. It is given by a linear combination of the first and second invariants,

$$W = C_1(I_1 - 3) + C_2(I_2 - 3), \tag{11}$$

and allows for a more accurate characterization of shear deformations, which are particularly important in incompressible, soft materials. The constants C_1 and C_2 are material constants determined empirically to fit the experimental data. From a microstructural point of view, the introduction of I_2 reflects contributions of chain interactions when they are constrained within a tube-like region around the molecular chains when they are stretched [12].

3 Theoretical considerations

3.1 The G-model

Here, in contrast to the classical approach of introducing the second invariant, I_2, as a means to improve the data fit of a generalised neo-Hookean model, we consider the extreme case of materials that *only* depend on I_2, that we refer to, for lack of a better name, as the *G-model*:

$$W = w(I_2), \tag{12}$$

the simplest one of which is the *linear G-model*, $W = C_2(I_2 - 3)$, which was first introduced by Hill in 1973 under the name *extreme-Mooney material*. For these materials, Hill showed that there are new exact solutions that can be expressed in terms of Bessel functions [15]. The only other G material that we know of is the incompressible Blatz-Ko model originally introduced to describe elastomeric foams [**?**].

3.2 Homogeneous deformations

3.2.1 Uniaxial tension and compression

Simple extension refers to a deformation applied to a material, where a uniaxial load is exerted along one principal axis, typically elongating the material in that direction while contracting it in the perpendicular directions due to the Poisson effect. This deformation is characterized by a stretch ratio, λ, where $\lambda > 1$ denotes uniaxial tension and $\lambda < 1$ denotes uniaxial compression. In the context of a rectangular block, this deformation can be described by

$$x_1 = \lambda X_1, \quad x_2 = \lambda^{-1/2} X_2, \quad x_3 = \lambda^{-1/2} X_3, \tag{13}$$

where, as before, x_i and X_i represent the coordinates in the deformed and reference configurations. Under this mode of deformation, we have $I_1 = \lambda^2 + 2/\lambda$ and $I_2 = 1/\lambda^2 + 2\lambda$, and $I_3 = 1$ and the axial stress T_{11} is

$$T_{11} = 2\left(\lambda^2 - \frac{1}{\lambda}\right)\left(W_1 + \frac{W_2}{\lambda}\right). \tag{14}$$

where we use the shorthand notation

$$W_1 = \frac{\partial W}{\partial I_1}, \quad W_2 = \frac{\partial W}{\partial I_2} \tag{15}$$

Therefore, for the G-model we have

$$T_{11} = 2w'(I_2)(\lambda - \frac{1}{\lambda^2}). \tag{16}$$

Close to the undeformed reference state, $\lambda = 1$, we recover a Hookean behaviour by linearizing this law to obtain the Young's modulus

$$E = \left.\frac{\partial T_{11}}{\partial \lambda}\right|_{\lambda=1} = 6w'(3). \tag{17}$$

Interestingly, for the linear law, we obtain the simple relationship $E = 6C_2$, and conclude that we can describe a Hookean behaviour without explicit dependence on the neo-Hookean term, i.e., entirely with out a dependence on the first invariant I_1.

It is of interest to compare the asymmetric behaviour in tension and compression between the GnH and G models. Starting with the linear case, we compare the two models by imposing that they have the same linear behavior close to the undeformed state, $\lambda = 1$. To illustrate the asymmetry between tension and compression, we display the asymmetry coefficient in Fig. 1,

$$a(\epsilon) = -T_{11}(1 + \epsilon) - T_{11}(1 - \epsilon) \tag{18}$$

and conclude that the linear G model displays a much stronger anisotropy than the GnH model. This asymmetry between tension and compression is also present in the general models. Indeed,

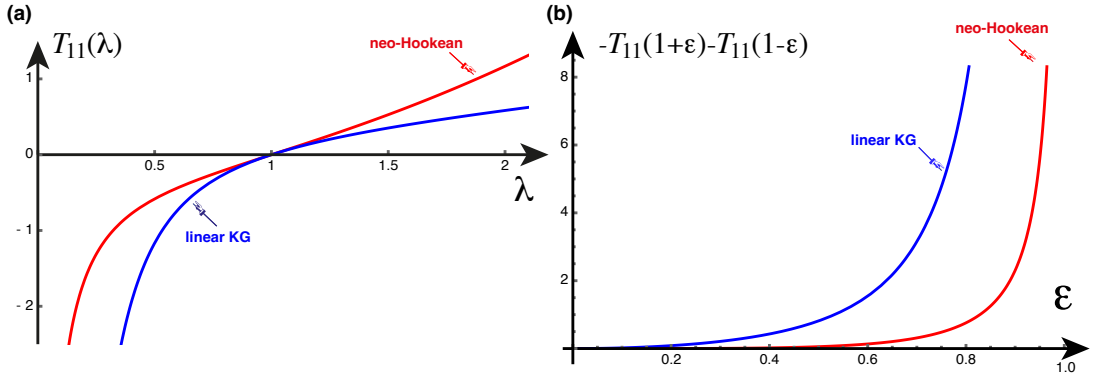

Figure 1: (a) Tension vs stretch for the neo-Hookean (red) and linear G model (blue), showing that for the same Young's modulus, the linear G model is softer in extension and stiffer in compression than the corresponding neo-Hookean model. (b) The asymmetry coefficient as a function of the strain shows a much larger asymmetry for the linear G model.

a series expansion around $\lambda = 1$ reveals the following behaviour for the GnH and G models:

$$T_{11}^{\mathrm{GnH}} = -E(\lambda-1) + \mathcal{O}((\lambda-1)^3), \quad a^{\mathrm{GnH}} = 0 + \mathcal{O}(\epsilon^3), \tag{19}$$

$$T_{11}^{\mathrm{G}} = -E(\lambda-1) - E(\lambda-1)^2 + \mathcal{O}((\lambda-1)^3), \quad a^{\mathrm{G}} = 2E\epsilon^2 + \mathcal{O}(\epsilon^3), \tag{20}$$

from which we conclude that G models are better suited to describe materials with a strong asymmetry between tension and compression as found in soft tissues, see Section **??**.

3.2.2 Triaxial deformations

Triaxial homogeneous deformations are characterized by an independent and uniform stretching along three mutually perpendicular axes, usually corresponding to the principal material directions. These deformations are described by the stretches $\lambda_1, \lambda_2, \lambda_3$ along the X_1, X_2, and X_3 axes, respectively:

$$x_1 = \lambda_1 X_1, \; x_2 = \lambda_2 X_2, \; x_3 = \lambda_3 X_3. \tag{21}$$

For such deformations, the invariants are:

$$I_1 = \lambda_1^2 + \lambda_2^2 + \lambda_3^2, \tag{22}$$

$$I_2 = \lambda_1^{-2} + \lambda_2^{-2} + \lambda_3^{-2}. \tag{23}$$

The Cauchy stress tensor is then diagonal with components:

$$T_{11} = 2(\lambda_1^2 - \lambda_3^2)(W_1 + \lambda_1^2 W_2), \tag{24}$$

$$T_{22} = 2(\lambda_2^2 - \lambda_3^2)(W_1 + \lambda_2^2 W_2). \tag{25}$$

For G materials, the ratio of these two stresses provides a universal relation [6, 35, 38]

$$\frac{T_{11}}{T_{22}} = \frac{\lambda_2^2\left(\lambda_1^2 - \lambda_3^2\right)}{\lambda_1^2\left(\lambda_2^2 - \lambda_3^2\right)}. \tag{26}$$

Since this relation does not explicitly depend on the choice of $w = w(I_2)$, it can be used to test if the material is indeed a G material, independently of the functional form of w.

3.2.3 Simple shear

Simple shear is an isochoric, volume-preserving deformation, commonly used in the experimental characterization and theoretical study of material behavior. It is given by the deformation

$$x_1 = X_1 + kX_2,\ x_2 = X_2,\ x_3 = X_3 \tag{27}$$

where k represents the shear magnitude in the $X_1 - X_2$ plane, with the shear angle given by $\arctan(k)$. This deformation does not change the volume because it involves a sliding motion of material planes over one another without altering the distance between these planes along the X_3 axis. The deformation gradient is:

$$\mathbf{F} = \begin{bmatrix} 1 & k & 0 \\ 0 & 1 & 0 \\ 0 & 0 & 1 \end{bmatrix}, \tag{28}$$

such that I_1 and I_2 are identical, $I_1 = I_2 = 3 + k^2$, and the Cauchy stress tensor becomes

$$\mathbf{T} = \begin{bmatrix} 2k^2W_1 & 2k(W_1 + W_2) & 0 \\ 2k(W_1 + W_2) & -2k^2W_2 & 0 \\ 0 & 0 & 0 \end{bmatrix}. \tag{29}$$

We note that, since the two invariants are equal, a data set purely generated from simple shear testing can be fitted equally by a GnH or G model. Without additional data produced by loading that distinguishes between the two invariants, there is no possibility of distinguishing the two models. For G materials, the stress simplifies to

$$\mathbf{T} = \begin{bmatrix} 0 & 2kW_2 & 0 \\ 2kW_2 & -2k^2W_2 & 0 \\ 0 & 0 & 0 \end{bmatrix}, \tag{30}$$

the implication of which will become clear in the next sections.

3.2.4 Pure shear

Pure shear is defined by a Cauchy stress tensor $\mathbf{T}$, in Cartesian coordinates, of the form:

$$[\mathbf{T}] = \begin{bmatrix} 0 & T & 0 \\ T & 0 & 0 \\ 0 & 0 & 0 \end{bmatrix}, \tag{31}$$

where T is the magnitude of the shear stress acting in the $x_1 - x_2$ plane. It corresponds to the deformation

$$x_1 = aX_1 + \sqrt{b^2 - a^2}X_2,\ x_2 = bX_2,\ x_3 = cX_3 \tag{32}$$

where a, b, and c depend on the material model and are chosen such that $abc = 1$ for incompressibility.

Figure 2 illustrates the first and second invariants as functions of the stretch for the homogeneous deformations of incompressible uniaxial tension, equibiaxial tension, and pure shear. Clearly, both invariants display tension compression asymmetry. Interestingly, for the special case of incompressibility with $I_1 = \lambda_1^{+2} + \lambda_2^{+2} + \lambda_2^{+2}$ and $I_2 = \lambda_1^{-2} + \lambda_2^{-2} + \lambda_2^{-2}$, in the range $\lambda = [0.5, ..., 2.0$, the minima and maxima of the first and second invariants are identical, but for

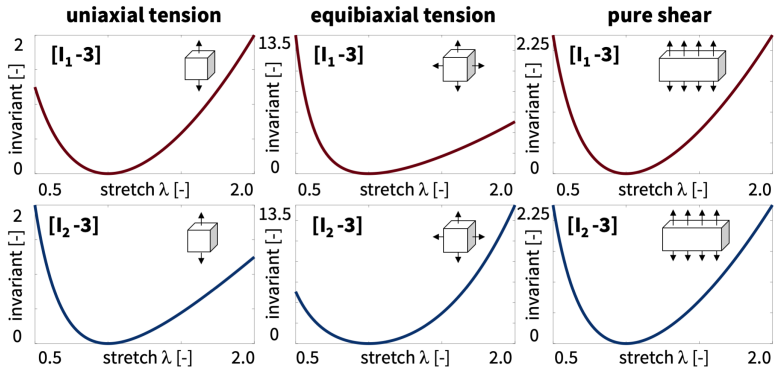

Figure 2: **Invariants as functions of stretch.** First invariant I_1, top row, and second invariant I_2, bottom row, as functions of the stretch λ for the homogeneous deformations of incompressible uniaxial tension, equibiaxial tension, and pure shear. Both invariants display tension compression asymmetry. For the special case of pure shear, both invariants are identical.

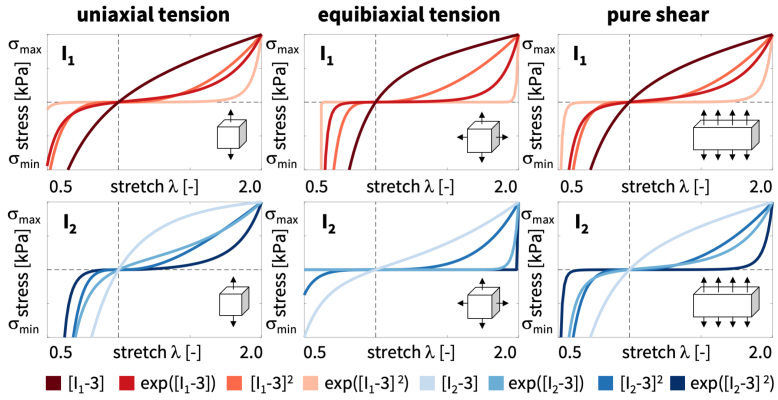

Figure 3: **Stresses as functions of stretch.** Stress components related to the first invariant I_1, top row, and second invariant I_2, bottom row, as functions of the stretch λ for the homogeneous deformations of uniaxial tension, equibiaxial tension, and pure shear. All stresses display tension compression asymmetry. For the special case of pure shear, the stress components are identical.

the special cases of uniaxial and equibiaxial tension, they occur under tension versus compression. For the special case of pure shear, both invariants are entirely identical.

Figure 3 illustrates the stresses as a function of the stretch for the homogeneous deformations of incompressible uniaxial tension, equibiaxial tension, and pure shear. The first and second rows display the stresses for first and second invariant models for the examples of a linear, $W = [I_{1,2} - 3]$, exponential linear, $W = \exp([I_{1,2} - 3]) - 1$, quadratic, $W = [I_{1,2} - 3]^2$, and exponential quadratic, $W = \exp([I_{1,2} - 3]^2) - 1$, free energy function. While the four functions are identical for both invariants for the special case of pure shear, they clearly differ under uniaxial and equibiaxial tension. Notably, the quadratic functions, $W = [I_{1,2} - 3]^2$ and $W = \exp([I_{1,2} - 3]^2) - 1$, have horizontal tangents at the origin and, when used alone without any additional terms, may result in complications, for example, in finite element analyses.

3.3 Inhomogeneous deformations

Finally, it is instructive to see how G materials respond for non-homogeneous deformations. Here we consider the example of the classical torsion problem [14, p. 333] where a long solid circular cylinder of radius A is subjected to a torsional deformation. Using cylindrical coordinates, where (R, Θ, Z) represents the position of a material point in the undeformed configuration and (r, θ, z) represents the same point in deformed configuration, the deformation is given by

$$r = R,\ \theta = \Theta + \tau Z,\ z = Z, \tag{33}$$

where τ is the twist per unit length. The Cauchy stress resulting from this torsional deformation is

$$\mathbf{T} = T_{rr}\mathbf{e}_r \otimes \mathbf{e}_r + T_{\theta\theta}\mathbf{e}_\theta \otimes \mathbf{e}_\theta + T_{zz}\mathbf{e}_z \otimes \mathbf{e}_z + T_{z\theta}\mathbf{e}_z \otimes \mathbf{e}_\theta, \tag{34}$$

where

$$T_{rr} = -\tau^2 \int_R^A rW_1(r)dr, \tag{35}$$

$$T_{\theta\theta} = -2\tau^2 \int_R^A rW_1(r)dr + 2\tau^2 R^2 W_1, \tag{36}$$

$$T_{zz} = -\tau^2 \int_R^A rW_1(s)dr - 2\tau^2 R^2 W_2, \tag{37}$$

$$T_{z\theta} = 2\tau R(W_1 + W_2), \tag{38}$$

where W_1 and W_2 are evaluated for the torsion problem at $I_1 = I_2 = 3 + \tau^2 R^2$.

The resultant moment M and axial force N required to maintain the deformation are determined by integrating the shear stress $T_{z\theta}$ and axial stress T_{zz} over the cross-sectional area of the cylinder, yielding:

$$M = \int_0^{2\pi} \int_0^A T_{z\theta} R^2 \,\mathrm{d}R\mathrm{d}\Theta = 4\pi\tau \int_0^A R^3(W_1 + W_2)\mathrm{d}R, \tag{39}$$

$$N = \int_0^{2\pi} \int_0^A T_{zz} R \,\mathrm{d}R\mathrm{d}\Theta = -2\pi\tau^2 \int_0^A R^3(W_1 + 2W_2)\mathrm{d}R. \tag{40}$$

For G materials, it follows that $N = -\tau M$. We also note the particularly simple form of the stress

$$T_{rr} = T_{\theta\theta} = 0,\ T_{zz} = -2\tau^2 R^2 W_2,\ T_{z\theta} = 2\tau R W_2, \tag{41}$$

which leads to another universal relation

$$T_{z\theta} = -\tau R\, T_{zz}. \tag{42}$$

We also conclude from (41) that no pressure develops on the side of the cylinder as it is twisted.

3.4 Inequalities

We recall that a fundamental set of inequalities are the Baker-Ericksen inequalities:

$$\lambda_i \neq \lambda_j \Rightarrow (t_i - t_j)(\lambda_i - \lambda_j) > 0, \quad \text{for} \quad i, j = 1, 2, 3, \tag{43}$$

where $\{t_1, t_2, t_3\}$ represent the principal stresses, the eigenvalues of $\mathbf{T}$, and, as before, $\{\lambda_1, \lambda_2, \lambda_3\}$ denote the principal stretches. These inequalities ensure that the direction of greater stretch corresponds to the direction of greater stress. The inequalities lead to restrictions on the choice of the model, traditionally written as [40, p. 171]:

$$\lambda_i^2 \lambda_j^2 \beta_1 > \beta_{-1}, \quad \text{if} \quad \lambda_i \neq \lambda_j, \tag{44}$$

$$\lambda_i^4 \beta_1 \geq \beta_{-1}, \quad \text{if} \quad \lambda_i = \lambda_j, \tag{45}$$

where the response functions for incompressible materials are given by

$$\beta_1 = 2W_1, \quad \beta_{-1} = -2W_2. \tag{46}$$

These conditions derived from the original inequalities are crucial for ensuring the non-negativity of the work done by stresses during deformation. In the context of pure shear, these inequalities ensure the expected behavior that the shear strains remain in the same direction as the applied shear force.

For G materials, we have $\beta_1 = 0$, and we see that both inequalities (44–45) imply

$$\beta_{-1} < 0, \quad \Rightarrow \quad \frac{\partial W}{\partial I_2} > 0, \tag{47}$$

which implies, from (17) that the Young modulus is also positive, as expected.

Finally, we also comment on the so-called empirical inequalities [40, p. 171] given by

$$\beta_1 > 0, \ \beta_{-1} \leq 0. \tag{48}$$

As their name suggests, These inequalities are not based on first principles and are inspired by observations of rubber-like materials. They are used to ensure that the constitutive model predicts realistic responses under various loading conditions. These conditions are sufficient to ensure that a tensile load leads to an extension, as expected [5]. However, these conditions are not necessary as we showed in Section 3.2.1. Further, it has also been established that these inequalities are not suitable for soft tissues [27]. Hence it is no surprise that for G materials the first inequality is not satisfied.

3.5 The Poynting effect

The Poynting effect in the context of simple shear deformation, is defined as the occurrence of normal stresses in the direction perpendicular to the shear plane. When a material undergoes simple shear deformation given by (27), the Cauchy stress tensor $\mathbf{T}$ may exhibit non-zero off-diagonal shear stress components as well as diagonal normal stress components [8, 34].

The Poynting effect refers to a situation where the normal stress components $T_{11} \neq T_{22}$. A *positive Poynting effect* is observed if $T_{22} < 0$, implying that the material experiences a compressive normal stress in the x_2 direction due to the shearing action, and the sheared faces of the material tend to 'spread apart'. Conversely, *a negative Poynting effect* [17, 27] is characterized by $T_{22} > 0$, where a tensile normal stress develops in the x_2 direction, causing the sheared faces to 'draw together'.

The implication of the Poynting effect extends to the expected behavior under pure shear stress, where the difference in shear stress $T = (\beta_1 - \beta_{-1})k$ is linked to either positive or negative Poynting effects.

For G materials, we have from (47) that $T_{22} < 0$ in simple shear. Hence we conclude that all G materials exhibit the positive Poynting effect, which is not always observed for soft tissues [9, 29] and suggests that such models may not be universally suitable for all soft tissues.

4 Data analysis

The burgeoning field of automated model discovery presents a transformative approach to constitutive modeling, using the power of neural networks to decipher complex material behaviors from expansive datasets. Neural networks, in particular, have been identified as a robust tool for constitutive model discovery, capable of sifting through vast data troves to unearth models without a priori physical knowledge. Despite their prowess in data fitting, classical neural networks ignore the rich legacy of constitutive modeling [16], at times disregarding thermodynamic principles and established physical laws. As a result,they often fail to extrapolate beyond their training regime. They excel at numerical fitting yet fall short in providing interpretative insights into the physics they model. Here we will use model discovery inspired by constitutive artificial neural networks [21, 24]. These networks embed physics directly into the network architecture and discover models that are not only data-compliant but also physically grounded, especially when they are reverse-engineered from classical constitutive elements, trained on a diverse array of mechanical tests, and validated against the mechanical properties of soft tissues [22, 23, 25, 33]. As such, they offer an intuitive understanding and a clear physical interpretation of their parameters and provide an important step towards a truly autonomous discovery of physically motivated models [39, 32]. Specifically, in pursuit of constitutive models that conform to the foundational principles of material behavior, we use a family of first and second invariant models that inherently satisfy thermodynamic consistency, material objectivity [40], symmetry, incompressibility, constitutive restrictions, and polyconvexity [3],

$$\begin{aligned} W(I_1, I_2) = w_1 \, [\, I_1 - 3 \,] \;\; + w_{2,2} \, [\exp(\, w_{1,2} \, [\, I_1 - 3 \,] \;\;) - 1 \,] \\ + w_3 \, [\, I_1 - 3 \,]^2 + w_{2,4} \, [\exp(\, w_{1,4} \, [\, I_1 - 3 \,]^2 \,) - 1 \,] \\ + w_5 \, [\, I_2 - 3 \,] \;\; + w_{2,6} \, [\exp(\, w_{1,6} \, [\, I_2 - 3 \,] \;\;) - 1 \,] \\ + w_7 \, [\, I_2 - 3 \,]^2 + w_{2,8} \, [\exp(\, w_{1,8} \, [\, I_2 - 3 \,]^2 \,) - 1 \,] \, . \end{aligned} \tag{49}$$

This family of models consists of eight terms and represents a total of 2^8 =256 different models a total of twelve model parameters, with the classical neo Hookean and the Mooney Rivlin models and many other popular existing models as special cases. We use uniaxial tension, uniaxial compression, and simple shear tests from human brain tissue of the gray matter cortex [**?**] to discover the model and parameters that best explain the experimental data [**?**]. This allows us to directly compare the performance of first and second invariant models [**?**].

Figure 4 summarizes the discovered best-in-class one- and two-term models from all possible models in equation (49). Squares on the diagonal represent the eight one-term models: the linear, $[I_{1,2} - 3]$, exponential linear, $\exp([I_{1,2} - 3]) - 1$, quadratic, $[I_{1,2} - 3]^2$, and exponential quadratic, $\exp([I_{1,2}-3]^2)-1$, models in terms of the first and second invariants, I_1 and I_2, in rows and columns one through four and five through eight. Squares outside the diagonal represent the 28 two-term models with all possible combinations of any two of these eight terms. The color code indicates the quality of fit, ranging from dark blue for the best fit to dark red for the worst fit. Strikingly, for the best-in-class one-term models, all four second invariant models outperform the four first invariant models as we conclude from the blue-to-orange colors for the fifth to eights squares on the diagonal compared to the dark red colors for the first to fourth squares. Notably, the widely used neo Hookean model, $W = w_1 \, [I_1 - 3]$, has the worst fit of all one-term models, followed by the popular Demiray model, $W = w_{2,2} \, [\exp(\, w_{1,2} [\, I_1 - 3 \,]) - 1 \,]$.

Figures 5 and 6 illustrate the eight one-term first and second invariant models associated with the diagonal terms in Figure 4 in terms of the nominal stress as a function of stretch or shear strain. All eight one-term models struggle to fit all three experiments simultaneously and overestimate the tensile stresses, while underestimating the compression and shear stresses. In agreement with Figure 4, the second invariant models in Figure 6 provide a better fit to the data than the first invariant models in Figure 5.

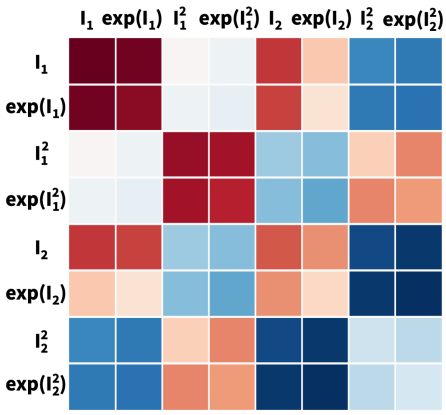

Figure 4: **Discovered best-in-class one- and two-term models for human brain.** Discovered one-term models, on the diagonal, and two-term models, off-diagonal, for model discovery with eight terms. Models are made up of eight functional building blocks: linear, exponential linear, quadratic, and exponential quadratic terms of the first invariant, rows and columns one through four, and of the second invariant, rows and columns five through eight. The color code indicates the quality of fit to human brain data, ranging from dark blue, best fit, to dark red, worst fit.

Figure 7 illustrates the discovered best-in-class two-term models associated with the dark blue o best-fit off-diagonal terms in Figure 4 in terms of the nominal stress as a function of stretch or shear strain. We note a significantly improved fit compared to the one-term models in Figures 5 and 6. The four best-in-class two-term models all combine the linear or exponential linear term $[I_2-3]$ or $\exp([I_2-3])-1$, with the quadratic or exponential quadratic term $[I_2-3]^2$ or $\exp([I_2-3]^2)-1$, strikingly, all in terms of the second invariant. Notably, the widely-used Mooney Rivlin model with linear terms in both invariants, $W = w_1\,[I_1-3] + w_5\,[I_2-3]$, is the third worst of all 28 two-term models. Taken together, the best-in-class two-term models in Figure 7 confirm the trend of the one-term models in Figures 5 and 6: For human brain tissue in tension, compression, and shear, second invariant models perform significantly better that first invariant models.

Lastly, Figure 8 illustrates the Poynting effect of the discovered best-in-class models for human brain. The top row highlights the best-in-class one-term models and the bottom row highlights the best-in-class two-term models. For all eight models, the load case of simple shear induces compressive stresses normal to the direction of shear. For models with linear terms, the Poynting effect is already visible at the zero-shear limit. For models with only quadratic terms, the Poynting has a horizontal tangent at the origin and only becomes visible for shear stresses on the order of 0.05. Importantly, none of the first invariant models can capture the Poynting effect–only the second invariant models display this characteristic behavior of lateral tension or compression when subjected to shear. Our algorithm automatically discovers second invariant models for gray matter tissue, suggesting that this is a relevant feature of human brain.

5 Conclusion

In the development of constitutive models for hyperelastic materials, the dependence on the first and second invariants I_1 and I_2 has been inspired by the statistical mechanics of long chain molecules. Early neo-Hookean models, derived from the assumption of Gaussian statistics of

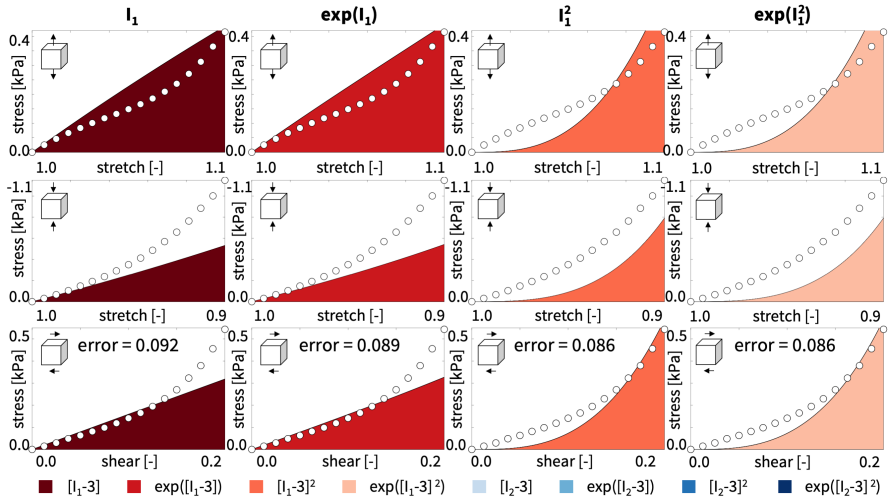

Figure 5: **Discovered one-term first invariant models.** Nominal stress as a function of stretch or shear strain for human gray matter tension, compression, and shear data. Circles represent the experimental data; color-coded regions represent the discovered terms for the linear, $W = [I_1 - 3]$, exponential linear, $W = \exp([I_1 - 3]) - 1$, quadratic, $W = [I_1 - 3]^2$, and exponential quadratic, $W = \exp([I_1 - 3]^2) - 1$, models; error value indicates the quality of fit.

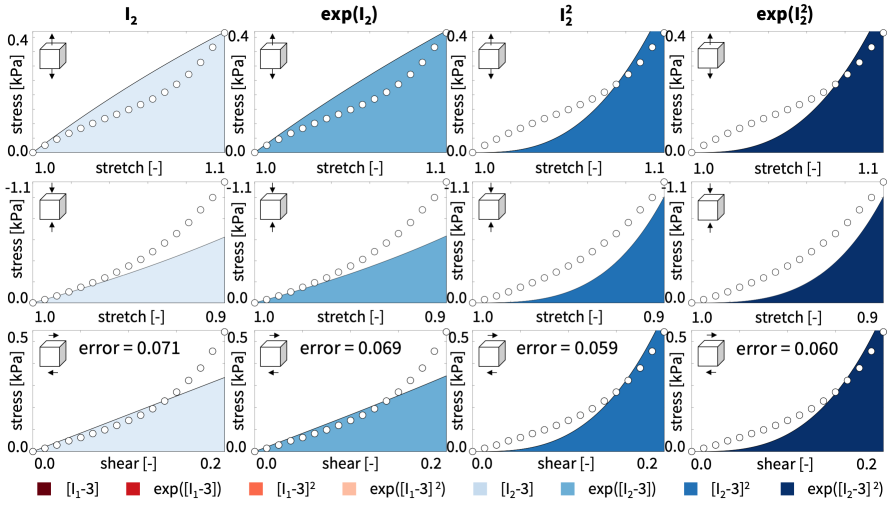

Figure 6: **Discovered one-term second invariant models.** Nominal stress as a function of stretch or shear strain for human gray matter tension, compression, and shear data. Circles represent the experimental data; color-coded regions represent the discovered terms for the linear, $W = [I_2 - 3]$, exponential linear, $W = \exp([I_2 - 3]) - 1$, quadratic, $W = [I_2 - 3]^2$, and exponential quadratic, $W = \exp([I_2 - 3]^2) - 1$, models; error value indicates the quality of fit.

chain configurations, were limited to terms dependent only on the first invariant I_1. However, we now recognize that such models can not adequately describe the experimentally observed material behavior, especially under finite deformations.

The introduction of I_2-dependent terms was motivated by the need to account for non-affine

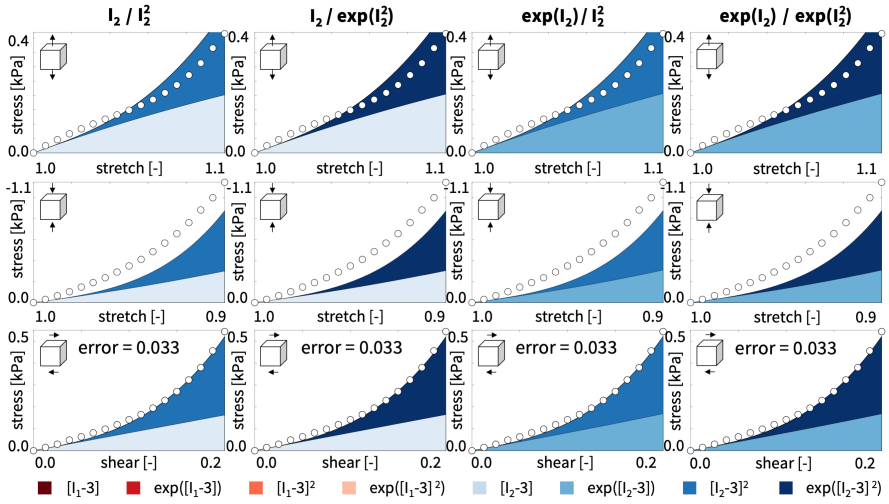

Figure 7: **Discovered best-in-class two-term models.** Nominal stress as a function of stretch or shear strain for human gray matter tension, compression, and shear data. Circles represent the experimental data; color-coded regions represent the discovered model terms; error value indicates the quality of fit.

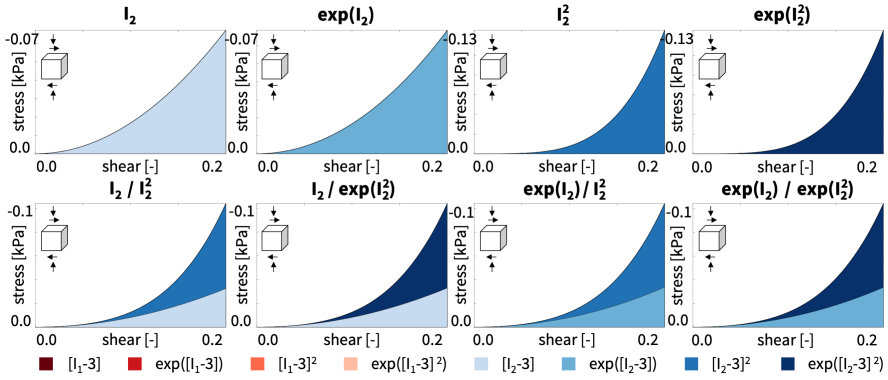

Figure 8: **Poynting effect for discovered best-in-class models.** Normal stress as a function of shear strain for the best-in-class one-term models, top row, and best-in-class two-term models, bottom row, for human gray matter shear data. Color-coded regions represent the discovered model terms.

deformations of the molecular chains, which the classical Gaussian models could not capture. In non-affine deformations, chains do not deform uniformly with the macroscopic strain, a situation commonly encountered in polymeric networks. Inclusion of the second invariant allows for the modeling of constraints imposed by neighboring chains and the resultant restriction on the non-affine deformation of the chains, a concept supported by the tube model of polymer dynamics. Hence, in addition to variations in chain length, these models also include variations of cross-sectional chain area [12, 36, 20].

6 Conclusions

Acknowledgments

It is our great pleasure to acknowledge helpful discussion and expertise from Giuseppe Saccomandi. The I-too-♥-I_2 movement started on 24 February at Il Fornaio, Palo Alto, and is now, very slowly, taking the world by storm.

References

[1] Amin Alibakhshi, Ali Imam, and Shahram Etemadi Haghighi. Effect of the second invariant of the cauchy–green deformation tensor on the local dynamics of dielectric elastomers. *International Journal of Non-Linear Mechanics*, 137:103807, 2021.

[2] Afshin Anssari-Benam, Andrea Bucchi, and Giuseppe Saccomandi. On the central role of the invariant i2 in nonlinear elasticity. *International Journal of Engineering Science*, 163:103486, 2021.

[3] S. S. Antman. *Nonlinear problems of elasticity*. Springer New York, 2005.

[4] AB Aydogdu, K Loos, M Johlitz, and A Lion. A new concept for the representative directions method: Directionalisation of first and second invariant based hyperelastic models. *International Journal of Solids and Structures*, 222:111017, 2021.

[5] RC Batra. Deformation produced by a simple tensile load in an isotropic elastic body. *Journal of Elasticity*, 6(1):109–111, 1976.

[6] M. F. Beatty. A class of universal relations in isotropic elasticity theory. *J. Elasticity*, 17(2):113–121, 1987.

[7] Millard F Beatty. An average-stretch full-network model for rubber elasticity. *Journal of Elasticity*, 70:65–86, 2003.

[8] E. W. Billington. The Poynting effect. *Acta Mech.*, 58(1):19–31, 1986.

[9] M Destrade, CO Horgan, and JG Murphy. Dominant negative poynting effect in simple shearing of soft tissues. *Journal of Engineering Mathematics*, 95:87–98, 2015.

[10] Michel Destrade, Jerry G Murphy, and Giuseppe Saccomandi. Simple shear is not so simple. *International Journal of Non-Linear Mechanics*, 47(2):210–214, 2012.

[11] Alexander Edmund Ehret and Alberto Stracuzzi. Variations on ogden's model: close and distant relatives. *Philosophical Transactions of the Royal Society A*, 380(2234):20210322, 2022.

[12] Eliot Fried. An elementary molecular-statistical basis for the mooney and rivlin–saunders theories of rubber elasticity. *Journal of the Mechanics and Physics of Solids*, 50(3):571–582, 2002.

[13] Y. B. Fu and R. W. Ogden. *Nonlinear Elasticity. Theory and Applications*. Cambridge University Press, Cambridge, 2001.

[14] A. Goriely. *The Mathematics and Mechanics of Biological Growth*. Springer Verlag, New York, 2017.

[15] James M Hill. Partial solutions of finite elasticity-three dimensional deformations. *Zeitschrift für angewandte Mathematik und Physik ZAMP*, 24:609–618, 1973.

[16] G. A. Holzapfel. Biomechanics of soft tissue. *The handbook of materials behavior models*, 3:1049–1063, 2001.

[17] CO Horgan and JG Murphy. Poynting and reverse poynting effects in soft materials. *Soft matter*, 13(28):4916–4923, 2017.

[18] Cornelius O Horgan and Michael G Smayda. The importance of the second strain invariant in the constitutive modeling of elastomers and soft biomaterials. *Mechanics of Materials*, 51:43–52, 2012.

[19] EA Kearsley. Note: Strain invariants expressed as average stretches. *Journal of Rheology*, 33(5):757–760, 1989.

[20] Martin Kroon. An 8-chain model for rubber-like materials accounting for non-affine chain deformations and topological constraints. *Journal of elasticity*, 102:99–116, 2011.

[21] Kevin Linka, Markus Hillgärtner, Kian P Abdolazizi, Roland C Aydin, Mikhail Itskov, and Christian J Cyron. Constitutive artificial neural networks: A fast and general approach to predictive data-driven constitutive modeling by deep learning. *Journal of Computational Physics*, 429:110010, 2021.

[22] Kevin Linka and Ellen Kuhl. A new family of constitutive artificial neural networks towards automated model discovery. *Computer Methods in Applied Mechanics and Engineering*, 403:115731, 2023.

[23] Kevin Linka, Sarah R St Pierre, and Ellen Kuhl. Automated model discovery for human brain using constitutive artificial neural networks. *Acta Biomaterialia*, 160:134–151, 2023.

[24] Kevin Linka, Nina Reiter, Jasmin Würges, Martin Schicht, Lars Bräuer, Christian J Cyron, Friedrich Paulsen, and Silvia Budday. Unraveling the local relation between tissue composition and human brain mechanics through machine learning. *Frontiers in bioengineering and biotechnology*, 9:704738, 2021.

[25] Kevin Linka, Adrian Buganza Tepole, Gerhard A Holzapfel, and Ellen Kuhl. Automated model discovery for skin: Discovering the best model, data, and experiment. *Computer Methods in Applied Mechanics and Engineering*, 410:116007, 2023.

[26] C Miehe, Serdar Göktepe, and F20965751091 Lulei. A micro-macro approach to rubber-like materials—part i: the non-affine micro-sphere model of rubber elasticity. *Journal of the Mechanics and Physics of Solids*, 52(11):2617–2660, 2004.

[27] L. A. Mihai and A. Goriely. Positive or negative Poynting effect? the role of adscititious inequalities in hyperelastic materials. *Proc. Roy. Soc. Lond. A*, 467(2136):3633–3646, 2011.

[28] L. A. Mihai and A. Goriely. Numerical simulation of shear and the Poynting effects by the finite element method: An application of the generalised empirical inequalities in non-linear elasticity. *Int. J. Nonlinear Mech.*, 49:1–14, 2012.

[29] L Angela Mihai, LiKang Chin, Paul A Janmey, and Alain Goriely. A comparison of hyperelastic constitutive models applicable to brain and fat tissues. *Journal of The Royal Society Interface*, 12(110):20150486, 2015.

[30] Melvin Mooney. A theory of large elastic deformation. *Journal of applied physics*, 11(9):582–592, 1940.

[31] R. W. Ogden. *Non-linear Elastic Deformations*. Dover, New york, 1984.

[32] Mathias Peirlinck, Kevin Linka, Juan A Hurtado, and Ellen Kuhl. On automated model discovery and a universal material subroutine for hyperelastic materials. *Computer Methods in Applied Mechanics and Engineering*, 418:116534, 2024.

[33] Sarah R St Pierre, Kevin Linka, and Ellen Kuhl. Principal-stretch-based constitutive neural networks autonomously discover a subclass of ogden models for human brain tissue. *Brain Multiphysics*, 4:100066, 2023.

[34] John Henry Poynting. On pressure perpendicular to the shear planes in finite pure shears, and on the lengthening of loaded wires when twisted. *Proceedings of the Royal Society of London. Series A, Containing Papers of a Mathematical and Physical Character*, 82(557):546–559, 1909.

[35] E. Pucci and G. Saccomandi. On universal relations in continuum mechanics. *Continuum Mech. Therm.*, 9(2):61–72, 1997.

[36] G Puglisi and G Saccomandi. Multi-scale modelling of rubber-like materials and soft tissues: an appraisal. *Proceedings of the Royal Society A: Mathematical, Physical and Engineering Sciences*, 472(2187):20160060, 2016.

[37] R. S. Rivlin. Large elastic deformations of isotropic materials. IV. further developments of the general theory. *Philos. Trans. Roy. Soc. A*, 241(835):379–397, 1948.

[38] G. Saccomandi. Universal results in finite elasticity. *Nonlinear Elasticity: Theory and Applications*, 283:97, 2001.

[39] Vahidullah Taç, Kevin Linka, Francisco Sahli-Costabal, Ellen Kuhl, and Adrian Buganza Tepole. Benchmarking physics-informed frameworks for data-driven hyperelasticity. *Computational Mechanics*, 73(1):49–65, 2024.

[40] C. Truesdell and W. Noll. *The Non-Linear Field Theories of Mechanics*. Springer, 2004.